This manuscript is now published at: https://doi.org/10.1016/j.epsl.2021.117161

This is the final authors version; this manuscript is now published in Earth and Planetary Science Letters. Please cite the published version: https://doi.org/10.1016/j.epsl.2021.117161

This manuscript is now published at: https://doi.org/10.1016/j.epsl.2021.117161

The stabilizing effect of high pore-fluid pressure along subduction megathrust faults: Evidence from friction experiments on accretionary sediments from the Nankai Trough

John D. Bedford[1,2], Daniel R. Faulkner[1], Michael J. Allen[1] and Takehiro Hirose[2]

[1]Rock Deformation Laboratory, Department of Earth, Ocean and Ecological Sciences, University of Liverpool, Liverpool, L69 3GP, UK

[2]Kochi Institute for Core Sample Research (X-star), Japan Agency for Marine-Earth Science and Technology (JAMSTEC), 200 Monobe-otsu, Nankoku, Kochi 783-8502, Japan

Corresponding author: John Bedford (jbedford@liverpool.ac.uk)

Highlights

- Nankai accretionary sediments exhibit strong rate-strengthening friction behaviour
- Frictional stability increases at high pore-fluid pressure: more rate-strengthening
- Effective normal stress at constant pore pressure has minimal effect on stability
- Elevated pore-fluid pressure may promote slow- or aseismic slip in subduction zones

This manuscript is now published at: https://doi.org/10.1016/j.epsl.2021.117161

Abstract

Pore-fluid pressure is an important parameter in controlling fault mechanics as it lowers the effective normal stress, allowing fault slip at lower shear stress. It is also thought to influence the nature of fault slip, particularly in subduction zones where areas of slow slip have been linked to regions of elevated pore-fluid pressure. Despite the importance of pore-fluid pressure on fault mechanics, its role on controlling fault stability, which is determined by the friction rate parameter $(a - b)$, is poorly constrained, particularly for fault materials from subduction zones. In the winter of 2018-19 the accretionary complex overlying the Nankai Trough subduction zone (SW Japan) was drilled as part of Integrated Ocean Drilling Program (IODP) Expedition 358. Here we test the frictional stability of the accretionary sediments recovered during the expedition by performing a series of velocity-stepping experiments on powdered samples (to simulate fault gouge) while systematically varying the pore-fluid pressure and effective normal stress conditions. The Nankai gouges, despite only containing 25% phyllosilicates, are strongly rate-strengthening and exhibit negative values for the rate-and-state parameter b. We find that for experiments where the effective normal stress is held constant and the pore-fluid pressure is increased the Nankai gouges become more rate-strengthening, and thus more stable (an increase in $(a - b)$ of ~6×10^{-5} MPa^{-1} with increasing pore-pressure). In contrast, when the pore-fluid pressure is held constant and the effective normal stress is varied, there is minimal effect on the frictional stability of the gouge. The increase in frictional stability of the gouge at elevated pore-fluid pressure is caused by an evolution in the rate-and-state parameter b, which becomes more negative at high pore-fluid pressure. These results have important implications for understanding the nature of slip in subduction zones and suggest the stabilizing effect of pore-fluid pressure could promote slow slip or aseismic creep on areas of the subduction interface that might otherwise experience earthquake rupture.

1. Introduction

Seismicity in subduction zones can result in megathrust earthquakes, the largest earthquakes in the world, often generating devastating tsunamis which pose a significant threat to human life and infrastructure in nearby coastal communities. Understanding the nature of the systems that produce these earthquakes, and the fault zones from which they arise, is therefore paramount in the mitigation of damage and loss of human life in future events. The Nankai Trough subduction zone lies off the coast of southwest Japan, with records of creep, slow-slip events and megathrust earthquakes occurring on the fault dating back over 1000 years (Ando, 1975). In the winter of 2018-19 the accretionary complex that overlies the Nankai megathrust was drilled, with cuttings and core samples collected, to a maximum depth of 3262.5 mbsf (meters below seafloor) at Integrated Ocean Drilling Program (IODP) Site C0002 during Expedition 358 (Tobin et al., 2020), as part of the Nankai Trough Seismogenic Zone Experiment (NanTroSEIZE) (Tobin and Kinoshita, 2006). Here we experimentally test the frictional properties of the materials recovered during Expedition 358. We investigate how the frictional stability, which is determined by the rate-and-state parameter $(a-b)$, is dependent on the effective normal stress conditions by performing a series of experiments at a range of different pore-fluid pressure and normal stress combinations. The aim of these experiments is not to necessarily mimic the stress conditions found on the subduction interface in nature, but rather to identify the relative contributions of pore-fluid pressure and normal stress to the constitutive frictional behaviour of the Nankai accretionary sediments (see section 1.2). Understanding the contributions of the different parameters in the effective stress law on the frictional stability, particularly pore-fluid pressure which can approach lithostatic pressures in subduction zones (Kodaira et al., 2004; Saffer and Tobin, 2011), is important for elucidating how different modes of fault slip, whether it be aseismic creep, slow-slip or earthquake rupture, may occur along the subduction interface.

1.1. Geological setting of the Nankai Trough and experimental samples

The Nankai Trough is located off the coast of southwest Japan (Fig. 1), where the Philippine Sea plate is subducted beneath the Eurasian plate at a rate of ~4-6 cm/yr (Seno et al., 1993). There is a long documented history of great earthquakes (with moment magnitude M_w >8.0) along the Nankai Trough, with recurrence intervals of ~90-150 years, and events often occurring in pairs, the most recent of which are the 1944 Tonankai (M_w 8.1) and the 1946 Nankaido (M_w 8.3) earthquakes (Ando, 1975). The 1944

This manuscript is now published at: https://doi.org/10.1016/j.epsl.2021.117161

event also produced a large tsunami, leading to widespread damage and loss of life along coastal areas of southwest Japan, that is thought to have been generated by earthquake rupture along a steeply-dipping splay fault branching up from the main subduction interface and cutting through the overlying accretionary prism (Park et al., 2002). As well as tsunamigenic earthquakes, a range of other fault slip behaviours have been observed in the Nankai Trough, including slow-slip events (Araki et al., 2017; Kodaira et al., 2004) and very low-frequency earthquakes (Ito and Obara, 2006; Sugioka et al., 2012), highlighting the variety of fault slip modes that occur in subduction zones.

The Nankai accretionary prism, which overlies the main subduction interface, consists of hemipelagic sediments that have been scraped off the subducting Philippine plate, and can be divided into the inner and outer wedges (Fig. 1b) which are separated by megasplay faults (Kimura et al., 2007). Previous NanTroSEIZE expeditions have drilled across the accretionary prism at various localities including the frontal thrust, the megasplay fault and into the overlying Kumano forearc basin (e.g. Kinoshita et al., 2009). Site C0002 is located in the inner accretionary prism above the main megathrust at a depth of ~5200 mbsf (Fig. 1b). This site was first drilled as part of IODP Expeditions 326, 338 and 348, and extended during Expedition 358 to a depth of 3262.5 mbsf (Kitajima et al., 2020). The samples used for experiments in this study are from drill cuttings recovered during this most recent extension of C0002, from a depth interval of 3212.5-3217.5 mbsf. At this depth the accretionary sediments primarily consist of silty claystone with minor amounts of fine-grained sandstone, siltstone and fine silty-claystone (Kitajima et al., 2020). Only cuttings from this depth interval were used in this study as we intend to investigate the role of varying pore-fluid pressure and effective normal stress on frictional stability, therefore we want to minimise the effects of any sample variability that might occur by using samples recovered from different depth intervals. Although it should be noted that these lithologies are typical of those found throughout the accretionary wedge system (Tobin et al., 2020) and we expect similar lithologies to be present along the main megathrust at seismogenic depths.

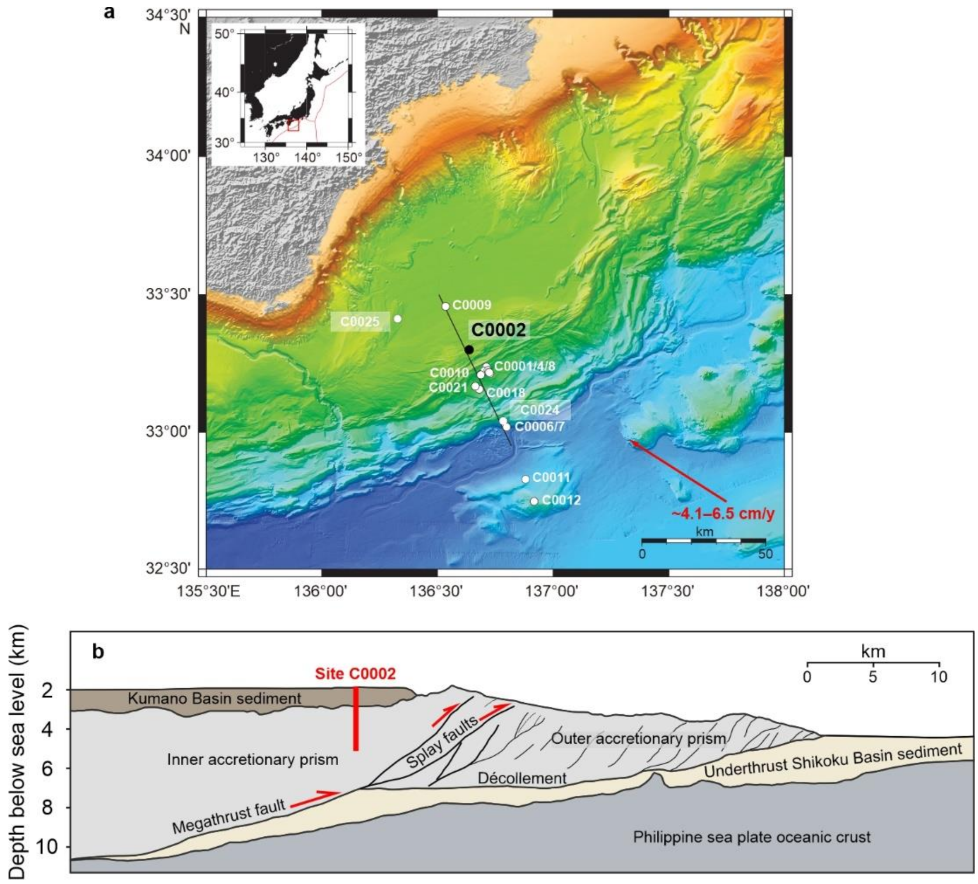

***Figure 1**: **a)** Bathymetric map of the Nankai Trough (modified from Tobin et al., (2020)) showing the NanTroSEIZE transect and drill sites of previous expeditions (white dots). The location of Site C0002 is shown as a black dot. **b)** Interpreted cross-section of the NanTroSEIZE transect (modified from Tobin et al., (2020)) showing Site C0002 which penetrated through the Kumano Basin and into the inner accretionary prism above the plate boundary megathrust fault.*

1.2. The roles of effective normal stress and pore-fluid pressure on fault stability

The roles of effective normal stress and pore-fluid pressure on fault friction are typically considered together using the effective stress law ($\sigma_n' = \sigma_n - \alpha P_f$), where the effective normal stress (σ_n') is equal to the normal stress (σ_n) minus the pore-fluid pressure (P_f) multiplied by the effective pressure coefficient (α). For most brittle materials it is typically considered that $\alpha \approx 1$ (Terzaghi, 1943), meaning that changes in either the pore-fluid pressure or the normal stress will have an equal effect on friction. As the apparent friction coefficient (μ), the ratio of shear stress (τ) to effective normal stress ($\mu =$

τ/σ_n'), of most geological materials is relatively constant over a wide range of effective normal stresses (Byerlee, 1978), any increase in pore-fluid pressure will thus allow fault slip to occur at lower shear stress. However, this does not dictate whether seismic (unstable) or aseismic (stable) slip will occur. Instead, the stability of fault slip is controlled by the rate-dependence of slip, derived from the rate-and-state constitutive relations for frictional sliding (e.g. Dieterich, 1979; Marone, 1998; Scholz, 1998). The rate-dependence of slip is described by the friction parameter $(a - b)$:

$$(a - b) = \Delta\mu_{ss}/\Delta lnV \qquad (1)$$

where μ_{ss} is the steady-state friction coefficient and V is the sliding velocity. When $(a - b)$ is positive then the sliding behaviour is rate-strengthening (μ_{ss} increases as V increases) and stable slip will prevail. In contrast, negative values of $(a - b)$ are associated with rate-weakening behaviour and are a prerequisite for unstable slip. Whether unstable slip will occur in rate-weakening materials is also dependent on the critical stiffness (k_c), given by the equation:

$$k_c = \frac{-(a-b)\sigma_n'}{D_c} \qquad (2)$$

where D_c is the characteristic slip weakening distance (i.e., the slip distance required for friction to change in response to a step velocity change). If the system stiffness (k) is less than the critical stiffness ($k < k_c$) then slip can accelerate leading to unstable stick-slip behaviour (e.g. Dieterich, 1979; Scholz, 1998). As can be seen in Equation 2, the effective normal stress, and thus also pore-fluid pressure, already exert an important control on fault stability. Low σ_n' (possibly as a result of high P_f) will cause a reduction in k_c which will stabilize the fault. However, it is not well understood what effect, if any, P_f has on the rate-dependence of slip, $(a - b)$. The aim of this study is therefore to investigate the roles of P_f and σ_n' on $(a - b)$ for Nankai accretionary materials.

There have been several previous experimental investigations into the rate-dependence of different fault materials, where either the effective normal stress and/or pore-fluid pressure have been varied. Although distinguishing the roles of σ_n' and/or P_f on the rate-dependence of slip is commonly not the primary aim of these previous investigations, we have collated σ_n' and P_f trends from these datasets in Table 1. We report the range of σ_n' and P_f test conditions for each study and the range of $(a - b)$ values recorded. We also note any relationships between σ_n', P_f and $(a-b)$, and whether they are positive (i.e., as σ_n' or P_f increase, $(a-b)$ increases) or negative (as σ_n' or P_f increase, $(a-b)$ decreases). Firstly if we consider the relationships between σ_n' and $(a-b)$, some gouges from natural fault zones show a positive relationship (e.g. Kurzawski et al., 2018, 2016; Smith and Faulkner, 2010) whereas others show a negative relationship (e.g. Carpenter et al., 2015, 2012; Rabinowitz et al., 2018). This contrast is likely due to differences in the gouge compositions, highlighted further by studies on synthetic gouges where the composition is controlled. For example quartz gouges typically show a negative relationship between σ_n' and $(a-b)$ (Mair and Marone, 1999; Marone et al., 1990), whereas carbonate (Scuderi et al., 2013; Scuderi and Collettini, 2016) and smectite gouges (Saffer et al., 2001; Saffer and Marone, 2003) often show positive relationships. It should be noted, however, that although smectite shows a positive relationship between σ_n' and $(a-b)$, many other phyllosilicate minerals show no relationship (Table 1).

Compared to studies investigating the role of σ_n', there are relatively few where the role of P_f alone on $(a-b)$ has been investigated. This requires experiments where σ_n' is kept constant while P_f is systematically varied. Experiments on the input sediments to the Middle America Trench suggest that P_f has a positive relationship with $(a-b)$ (Kurzawski et al., 2018, 2016). In contrast, fluid-injection experiments on calcite gouge suggest that P_f has a negative relationship with $(a-b)$ (Scuderi and Collettini, 2016). The study of Scuderi and Collettini, (2016) nicely replicates the evolving stress conditions that occur in nature, which is important for understanding processes associated with induced seismicity; however both P_f and σ_n' are changing in these experiments meaning it is difficult to constrain the individual contributions of each parameter on $(a-b)$. In this study we aim to expand on the previous works of Scuderi and Collettini (2016) and Kurzawski et al., (2018, 2016) by performing experiments to identify the individual contributions of P_f and σ_n' on $(a-b)$ for Nankai accretionary materials. Other variables have also been shown to influence the rate-dependence of friction including temperature (Okamoto et al., 2020; Sawai et al., 2016), sliding velocity (Carpenter et al., 2016; Ikari et al., 2009a; Saffer and Marone, 2003) and gouge composition (den Hartog and Spiers, 2013), demonstrating that care must be taken when interpreting rate-and-state data from experiments where multiple parameters have been varied. Xing et al., (2019) independently investigated the role of P_f on the frictional rate-dependence of quartz, olivine, antigorite and chrysotile gouges and found a positive relationship between P_f and $(a - b)$, with antigorite exhibiting the strongest positive relationship, which they explain by a dilatant hardening mechanism in the gouge. In this study we aim to test if the P_f relationships observed by Xing et al., (2019) also occur in clay-bearing materials from a subduction zone. Understanding the role of variable pore-fluid pressure on frictional rate-dependence is important in subduction zone settings as P_f is likely to be heterogeneously distributed along the subduction interface (Hirose et al., 2021) and the occurrence of slow earthquakes is often associated with regions of elevated P_f (e.g. Kodaira et al., 2004; Warren-Smith et al., 2019), suggesting that pore-fluid pressure may exert an important control on frictional stability in these tectonic settings.

Material	Study	σ'_n (MPa)	P_f (MPa)	$(a-b)$	$(a-b)$ relationship with $\overline{\sigma_n}$	$(a-b)$ relationship with P_f	Notes
Natural fault gouges:							
Hikurangi Trench (New Zealand)	**[1]**	1-150	0.5-15	-0.0028 to 0.021	Negative	Not reported	Calcareous mudstone input sediments
Middle America Trench (Co. Rica)	**[2,3]**	30-110	20-120	-0.015 to 0.023	Positive	Positive	Silty clay gouge
Panamint Valley Normal Fault (USA)	**[4]**	5-150	Dry (RH)	0.002 to 0.010	None	-	Quartz-feldspar-calcite-clay mixtures
San Andreas Fault (USA).	**[5,6]**	7-100	3-20	0.004 to 0.019	Negative	Not reported	CDZ (Saponite clay-quartz mixtures)
Zuccale Normal Fault (Italy)	**[7]**	20-150	13-240	-0.062 to 0.045	Complex	Complex	(a-b) dependent on σ'_n, P_f, temp. and vel.
Zuccale Normal Fault (Italy)	**[8]**	25-75	50	-0.001 to 0.007	Positive	-	Variable composition fault gouges
Quartz gouges:							
Quartz	**[9]**	25-75	Dry (RH)	-0.007 to 0.014	Neg. (weak)	-	Neg. at disp. >5 mm
Quartz	**[10]**	50-190	5 or 10	0.0017 to 0.0044	Negative	-	
Quartz	**[11]**	70	5-60	0.0025 to 0.0043	-	Positive (weak)	
Phyllosilicate-rich gouges:							
Chlorite	**[12]**	100-400	50-220	-0.009 to 0.016	None	None	Temp = 22-600°C
Chlorite	**[13]**	12-58	5	0.003 to 0.010	None	-	(a-b) is vel dependent
Illite	**[13]**	12-58	5	0.003 to 0.010	None	-	(a-b) is vel dependent
Illite	**[14]**	5-150	Dry (RH)	0.0015 to 0.0040	None	-	(a-b) is vel dependent
Illite-quartz	**[15]**	25-200	50-200	-0.023 to 0.037	Negative	Positive (weak)	Qtz-fract. dependent
Montmorillonite	**[13]**	12-58	5	0.001 to 0.006	None	-	(a-b) is vel dependent
Montmorillonite	**[16]**	10-70	10	-0.0017 to 0.0040	Negative	-	Temp = 25-150°C
Montmorillonite	**[17]**	10-700	Dry or 10	0.0002 to 0.009	Complex	-	
Smectite	**[14]**	5-150	Dry (RH)	-0.0030 to 0.0053	Positive	-	(a-b) is vel dependent
Smectite	**[18]**	5-50	Dry (RH)	-0.0025 to 0.0053	Positive	-	
Carbonate/evaporite gouges:							
Anhydrite-dolomite	**[19]**	10-150	Dry or 2	-0.0020 to 0.0039	Positive (weak)	-	
Calcite	**[20]**	1-100	Saturated	-0.005 to 0.013	None	-	(a-b) is vel dependent
Calcite	**[21]**	19-30	0-28	0 to 0.005	Positive	Negative	Fluid injection exps.
Talc-calcite	**[22]**	5-50	Saturated	0.0042 to 0.0107	None	-	
Other gouges:							
Actinolite-chlorite	**[23]**	50-200	50-200	-0.018 to 0.052	Positive (weak)	Positive (weak)	Temp. dependent
Antigorite	**[11]**	30 or 70	5-90	-0.0044 to 0.0094	-	Positive	
Blueschist	**[24]**	25-200	25-200	-0.03 to 0.03	Positive	-	$\sigma'_n/P_f = 0.5$
Brucite	**[25]**	10-60	Saturated	-0.0047 to 0.0012	Positive	-	
Chrysotile	**[11]**	70	5-60	0.0047 to 0.0072	-	Positive (weak)	
Olivine	**[11]**	70	5-60	0.0050 to 0.0064	-	Positive (weak)	

***Table 1**: Collation of previous data on different fault gouges where (a-b) has been measured as effective normal stress and/or pore-fluid pressure is varied. RH = room/ambient humidity. The reference studies listed are: **[1]** Rabinowitz et al., (2018), **[2,3]** Kurzawski et al., (2018, 2016), **[4]** Numelin et al., (2007), **[5,6]** Carpenter et al., (2015, 2012), **[7]** Niemeijer and Collettini (2014), **[8]** Smith and Faulkner (2010), **[9]** Mair and Marone (1999), **[10]** Marone et al., (1990), **[11]** Xing et al., (2019), **[12]** Okamoto et al., (2019), **[13]** Ikari et al., (2009a), **[14]** Saffer and Marone (2003), **[15]** den Hartog and Spiers (2013),*

***[16]** Mizutani et al., (2017) **[17]** Morrow et al., (2017), **[18]** Saffer et al., (2001), **[19]** Scuderi et al., (2013), **[20]** Carpenter et al., (2016), **[21]** Scuderi and Collettini (2016), **[22]** Giorgetti et al., (2015), **[23]** Okamoto et al., (2020), **[24]** Sawai et al., (2016), **[25]** Okuda et al., (2021).*

1.3. Previous investigations into the frictional behaviour of Nankai sediments

To investigate the roles of effective normal stress and pore-fluid pressure on $(a-b)$ we use samples collected from drilling of the Nankai Trough. Previous experimental studies on the frictional behaviour of materials collected from Nankai drilling have been performed at low effective normal stresses (≤25 MPa) and pore-fluid pressures (≤5 MPa). These studies have shown that at slow sliding velocities (0.03-100 $\mu m \cdot s^{-1}$) Nankai accretionary materials exhibit predominantly rate-strengthening behaviour (Ikari et al., 2009b; Ikari and Saffer, 2011), in agreement with other studies on clay-bearing gouge materials (e.g. Ikari et al., 2009a; Morrow et al., 2017). However rate-weakening behaviour has been reported for Nankai materials during experiments at low effective normal stress (5 MPa) (Tsutsumi et al., 2011), at ultra-low, plate-rate velocities (Ikari and Kopf, 2017), and for intact samples that have high cohesive strength (Roesner et al., 2020). Extreme dynamic weakening has also been observed in Nankai materials during experiments approaching seismic slip rates (1.3 ms^{-1}) as a result of thermally-activated weakening processes (Ujiie and Tsutsumi, 2010).

In this study we extend the range of previously investigated stress conditions on Nankai materials by conducting frictional sliding experiments at effective normal stresses of 10-75 MPa and pore-fluid pressures of 5-75 MPa (summarized in Table 2). By performing a series of velocity-stepping experiments across a range of pore-fluid pressure and effective normal stress conditions, we aim to determine the individual contributions of these parameters on the constitutive rate-dependent frictional behaviour, $(a-b)$, of the Nankai accretionary materials.

2. Methods

2.1. Sample preparation

Drill cuttings recovered from a depth interval of 3212.5-3217.5 mbsf were used for experiments. First, the cuttings were washed to remove any residue drilling mud before being left to dry in an oven at 60°C for 24 hours. Cuttings were then crushed and sieved to form a simulated gouge powder with a grain size of <125 µm, similar to sample preparation methodologies used in previous studies (e.g. Carpenter et al., 2015; Kurzawski et al., 2018; Rabinowitz et al., 2018).

X-ray Diffraction (XRD) analysis was used to determine the mineralogical composition of the simulated gouge. Representative sub-samples were crushed, in distilled water, to a powder <10 µm using an agate McCrone micronizing mill, and dried at 60°C. Dried samples were then crushed into a light and loose powder in an agate pestle and mortar before being back-loaded into a cavity holder as random powders. A copper X-ray tube was used, with a nickel filter to select for copper K-α radiation. Scans covered the range of 4-70° 2θ. To determine the presence of swelling clay (smectite) the powdered samples were saturated with ethylene glycol, by the vapour pressure method at 60 °C for 24 h and rescanned. Quantification of the mineralogy was achieved using the Relative Intensity Ratio (RIR) method (Hillier, 2000). XRD results showed the Nankai gouge to be comprised of quartz (49%), plagioclase (21%), illite (14%), K-feldspar (6%), chlorite (5%) and smectite (5%).

2.2. Experimental procedure

Gouge layers are sheared at ambient temperature in a direct-shear geometry (Fig. 2) within a conventional triaxial deformation apparatus (see Faulkner and Armitage, 2013). The gouge is measured by weight to produce a layer with an initial thickness of ~1 mm that is placed between direct-shear forcing blocks (e.g. Sánchez-Roa et al., 2017). Soft silicone spacers are positioned at each end to allow shear of the layer to be accommodated without supporting any load. Grooves (200 µm deep, with a 400 µm spacing) are cut into the sliding area (50 x 20 mm) on the forcing blocks, perpendicular to the shear direction, to ensure that shear occurs within the layer itself and not between the edges of the gouge and the forcing blocks. Once the layer is prepared the direct-shear assembly is wrapped in a low-friction PTFE sleeve (0.25 mm thickness) before being inserted into a 3 mm thick PVC jacket. The PTFE sleeve is used to minimize friction between the jacket and the direct-shear assembly in the vicinity of the layer. The jacketed direct-shear assembly is then positioned between the platens of the sample assembly and inserted into the pressure vessel of the triaxial apparatus. Normal stress is applied to the layer by the confining pressure, and pore-fluid pressure is introduced via three porous disks on each forcing block, spaced to ensure an even distribution of fluid (Fig. 2). Deionized water was used as the pore fluid in this study. Both the confining and pore-fluid pressures are held constant during an experiment by servo-controlled pumps attached to each pressure system, with a resolution of better than 0.05 MPa. The gouge layer is sheared by the axial piston and the applied force is measured via an internal force gauge with a measurement resolution of better than 0.05 kN. In this setup a maximum load-point displacement of 8.5 mm can be achieved, which equates to a shear strain (γ) of ~10, given the final layer thickness of ~0.85 mm.

This manuscript is now published at: https://doi.org/10.1016/j.epsl.2021.117161

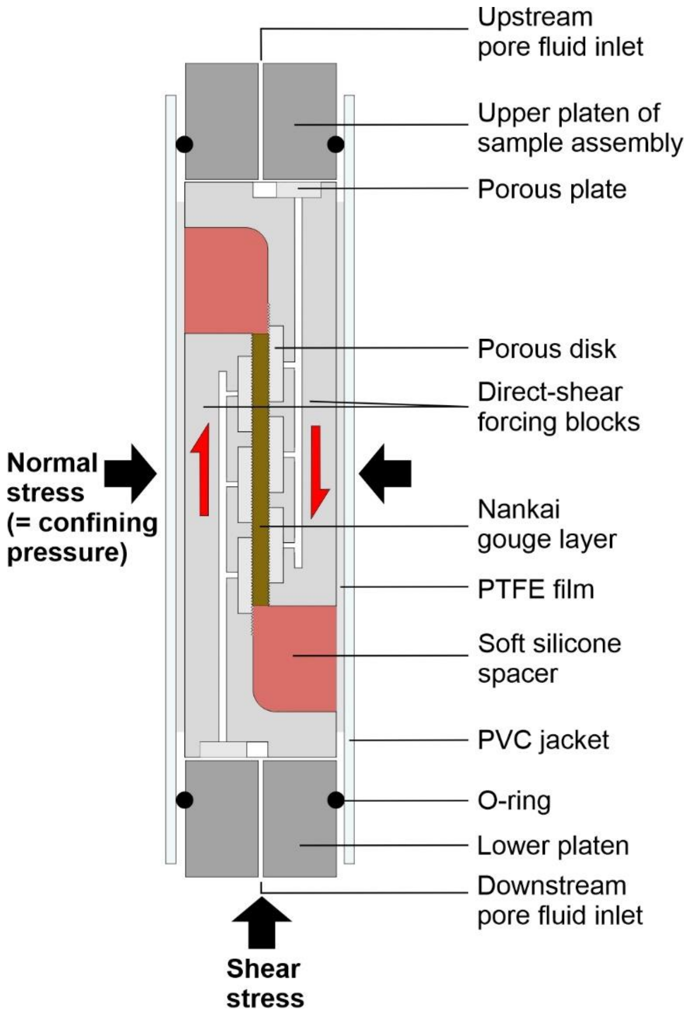

Figure 2*: An illustration of the direct-shear experimental set up (platen diameter is 20 mm). The assembly is placed into a triaxial deformation apparatus where the confining pressure applies the normal stress across the gouge layer. Pore-fluid pressure is servo-controlled at the boundaries of the layer through three sintered stainless steel porous disks on each direct-shear forcing block.*

Experiments were performed over a total of 20 different stress-conditions (Table 2), at four different effective normal stresses (10, 25, 50 and 75 MPa) and five different pore-fluid pressures (5, 10, 25, 50 and 75 MPa). For example, for an experiment performed at 75 MPa effective normal stress and 75 MPa pore-fluid pressure, the confining pressure (P_c) is 150 MPa ($\sigma_n' = P_c - P_f$). In each experiment the gouge layers were sheared for an initial 1.5 mm displacement at 0.3 μm·s^{-1}, before velocity steps of 0.3 to 3 μm·s^{-1} and back were applied every subsequent 1 mm of displacement to determine the rate-dependence of slip, $(a - b)$. Data were acquired at a logging frequency of 10 Hz for all tests in this study. The rate-and-state parameters, a and b, were determined by processing the velocity steps using the RSFit3000 program (Skarbek and Savage, 2019) which applies an inverse modelling technique with an iterative least-squares fit. The program also solves for D_c (reported in Supplementary Tables 1 and 2) and treats the stiffness as a fitting parameter.

At the end of each experiment the permeability of the gouge was measured using the transient pulse decay method (see Brace et al., 1968). This involves abruptly increasing P_f by approximately 0.5 MPa at the upstream end of the sample, producing a pressure differential across the gouge layer. This pressure differential then decays with time as the pore-fluid dissipates through the sample allowing for the permeability to be calculated. The transient pulse decay method has been shown previously to provide reliable permeability values consistent with other measurement techniques such as the pore pressure oscillation method (Faulkner and Rutter, 1998).

Experiment	σ_n' **(MPa)**	P_f **(MPa)**	P_c **(MPa)**	**λ** (P_f/σ_n)	**Velocity (μm·s^{-1})**
Nankai 1	10	5	15	0.33	0.3 - 3
Nankai 2	10	10	20	0.5	0.3 - 3
Nankai 3	10	25	35	0.71	0.3 - 3
Nankai 4	10	50	60	0.83	0.3 - 3
Nankai 5	10	75	85	0.88	0.3 - 3
Nankai 6	25	5	30	0.16	0.3 - 3
Nankai 7	25	10	35	0.28	0.3 - 3
Nankai 8	25	25	50	0.5	0.3 - 3
Nankai 9	25	50	75	0.67	0.3 - 3
Nankai 10	25	75	100	0.75	0.3 - 3
Nankai 11	50	5	55	0.09	0.3 - 3
Nankai 12	50	10	60	0.17	0.3 - 3
Nankai 13	50	25	75	0.33	0.3 - 3
Nankai 14	50	50	100	0.5	0.3 - 3
Nankai 15	50	75	125	0.6	0.3 - 3
Nankai 16	75	5	80	0.06	0.3 - 3
Nankai 17	75	10	85	0.12	0.3 - 3
Nankai 18	75	25	100	0.25	0.3 - 3
Nankai 19	75	50	125	0.4	0.3 - 3
Nankai 20	75	75	150	0.5	0.3 - 3

Table 2*: Summary of experiments performed in this study. The normal stress* (σ_n) *is provided by the confining pressure* (P_c)*. Also shown is the pore-fluid factor for each experiment* $(\lambda = P_f/\sigma_n)$.

3. Results

3.1. Frictional strength and behaviour

An example of a typical frictional sliding test is shown in Figure 3a. The gouge samples initially undergo quasi-elastic loading, shown by the steep increase in coefficient of friction, before yielding and the initiation of steady-state sliding at approximately 1 mm of load point displacement. The friction coefficient of the Nankai gouge at steady-state sliding is between 0.37-0.45 for all tests, with negligible cohesion (Fig. 3c). Note that the reported shear stress values in Figure 3c were taken at 1.5 mm displacement, after the initiation of steady-state slide and before the first velocity step in each test. The range of strength values is likely a result of sample variability as the coefficient of friction is independent of the effective normal stress and pore-fluid pressure conditions (Fig. 3c). This suggests that the mechanical (frictional) strength obeys the effective stress law ($\sigma_n' = \sigma_n - \alpha P_f$) and the effective pressure coefficient (α) for this parameter is approximately equal to 1.

The Nankai gouge exhibits strongly rate-strengthening frictional behaviour, with $(a - b)$ ranging from 0.0042 to 0.0219 across all tests in this study as σ_n' and P_f are varied. The majority of the velocity steps are characterised by negative b-values (Fig. 3b), which have been widely observed for other phyllosilicate-bearing gouges (Carpenter et al., 2015; Ikari et al., 2009a; Sánchez-Roa et al., 2017; Scuderi and Collettini, 2018; Smith and Faulkner, 2010). The Nankai gouge also exhibits an asymmetrical frictional response to up-steps and down-steps in the sliding velocity (Fig. 3b), with $(a - b)$ values determined from down-steps in the sliding velocity (3 to 0.3 $\mu m \cdot s^{-1}$) being greater (i.e. more rate-strengthening) than those determined from up-steps in the sliding velocity (0.3 to 3 $\mu m \cdot s^{-1}$). Similar asymmetrical responses have been reported previously (Rathbun and Marone, 2013; Xing et al., 2019) and are hypothesised to be related to differences in the grain-scale response of granular gouges to velocity increases and decreases (Rathbun and Marone, 2013).

This manuscript is now published at: https://doi.org/10.1016/j.epsl.2021.117161

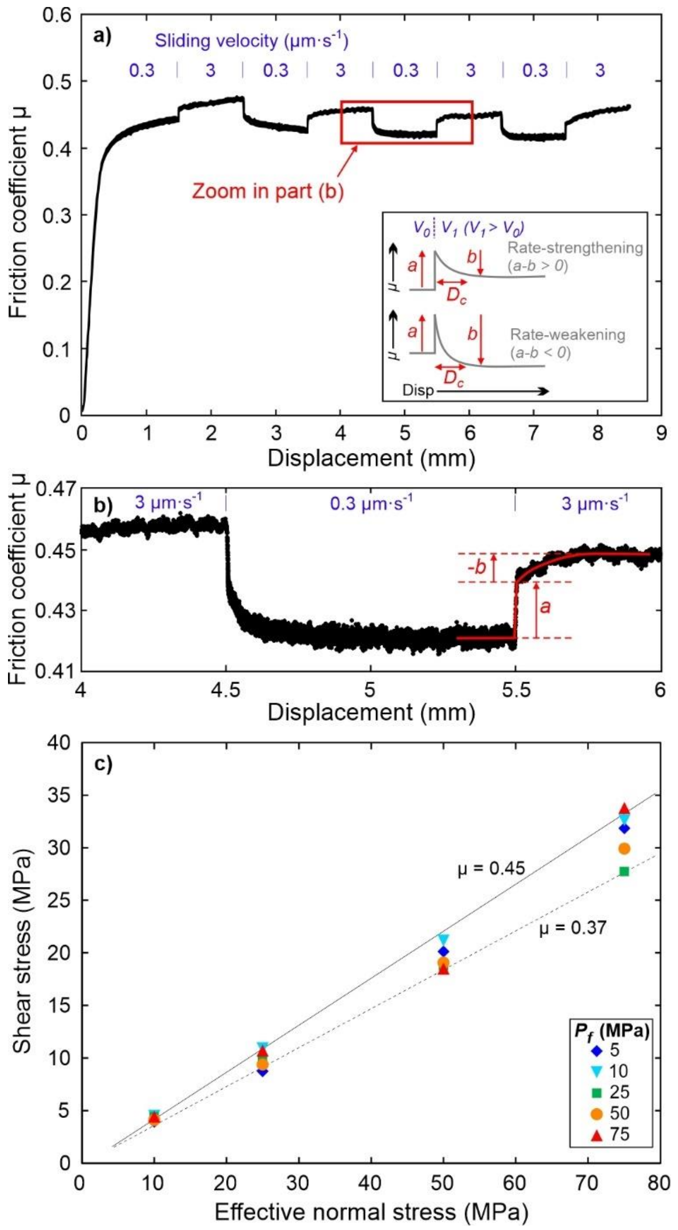

***Figure 3**: **a)** An example of a complete experiment (σ_n' = 25 MPa, P_f = 75 MPa) showing the evolution of the coefficient of friction with displacement as the sliding velocity is stepped between 0.3 and 3 μm·s^{-1}. The inset shows how the coefficient of friction typically evolves for rate-strengthening and rate-weakening materials, where the friction rate parameters a and b are both positive. **b)** A zoom on velocity steps from the experimental data on Nankai gouge, shown by the box in* (a), *highlighting the rate-strengthening nature of the gouge and the occurrence of negative b-values. **c)** Shear stress as a function of normal stress for all tests in this study. The reported shear stress values are after 1.5 mm displacement (just before the first velocity step).*

3.2. The roles of effective normal stress and pore-fluid pressure on the velocity dependence of friction

The $(a-b)$ values of the Nankai gouge are shown in Figure 4 as a function of (1) effective normal stress at constant pore-fluid pressure, and (2) pore-fluid pressure at constant effective normal stress. Note that only the $(a-b)$ values calculated from velocity up-steps (0.3 to 3 μm·s^{-1}) are shown, with the average up-step values for a given test shown in bold and connected by contours of equal σ_n' or P_f. At constant pore-fluid pressure, when $\sigma_n' \geq 25$ MPa, the $(a-b)$ values are largely independent of effective normal stress (Fig. 4a) and thus also independent of normal stress (σ_n). There is however, a decrease in $(a-b)$ at low effective normal stress (between 10 and 25 MPa effective normal stress). In contrast, at constant effective normal stress there is a systematic increase in $(a-b)$ with pore-fluid pressure, with the gouge becoming more rate-strengthening at elevated P_f (Fig. 4b). Again, there is a difference in the frictional behaviour between 10 and 25 MPa effective normal stress with no clear pore-fluid pressure dependence for tests conducted at σ_n' = 10 MPa.

The results collected at σ_n' = 10 MPa exhibit greater scatter and do not show as clear a trend as the tests when $\sigma_n' \geq 25$ MPa. Consequently, we have included this data with dashed lines so as to emphasise the clear trends in the results of the data. We discuss the possible reasons for the behaviour at $\sigma_n' = 10$ MPa later in the paper. The scatter we observe in the data at $\sigma_n' \geq 25$ MPa for individual experiments (i.e., the small datapoints in Fig. 4), can be explained by a slight displacement dependent evolution of $(a-b)$. In Supplementary Figure 1 we show how $(a-b)$ evolves for individual experiments as a function of net displacement; we find that $(a-b)$ increases slightly with increasing displacement (i.e., increasing shear strain). Similar displacement dependent behaviour has been reported previously, however this is mainly observed in rate-weakening materials that become more rate-weakening over comparable shear strains to our study (Beeler et al., 1996; Ikari et al., 2011; Mair and Marone, 1999; Scruggs and Tullis, 1998); here we observe the opposite phenomena where the rate-strengthening Nankai materials become more rate-strengthening with displacement. Despite the slight displacement dependence, the predominant control on $(a-b)$ for the Nankai accretionary materials in this study is the pore-fluid pressure (Fig. 4 and Supplementary Fig. 1).

This manuscript is now published at: https://doi.org/10.1016/j.epsl.2021.117161

As we have tested the rate-dependence of friction, $(a-b)$, of the Nankai gouge over a range of pore-fluid pressure and normal stress conditions, the data can also be plotted as a pore-fluid factor, λ (where $\lambda = P_f/\sigma_n$). The overall trend in this plot (Fig. 5) shows that as λ approaches 1 (i.e., as pore-fluid pressure approaches lithostatic pressure), $(a-b)$ increases. We have separated the data in the figure to highlight the P_f conditions of each experiment using the same legend as Figure 4a. This shows further that at constant pore-fluid pressure (i.e., varying normal stress) there is little change in $(a-b)$. In contrast, as P_f is increased $(a-b)$ also increases; this is clearly shown when looking at the data for experiments performed at pore-fluid pressures of 25, 50 and 75 MPa when λ = 0.5 (Fig. 5). The data in Fig. 5 therefore support the pore-pressure dependence on $(a-b)$ observed in Fig. 4, although Fig. 4 highlights better the individual contributions of P_f and σ_n' on the frictional rate-dependence.

The pore-pressure dependence on $(a-b)$ that we observe for tests conducted at $\sigma_n' \geq 25$ MPa on Nankai gouge is similar to that observed by Xing et al., (2019) for antigorite gouge. For example in our data, when $\sigma_n' = 75$ MPa, the average up-step $(a-b)$ value increases from 0.00645 at $P_f = 5$ MPa, to 0.01053 at $P_f = 75$ MPa. This corresponds to a ~6×10^{-5} MPa^{-1} increase in $(a-b)$ with increasing pore-fluid pressure, which is similar to the ~5×10^{-5} MPa^{-1} increase in $(a-b)$ with pore-fluid pressure reported by Xing et al., (2019) for antigorite gouge.

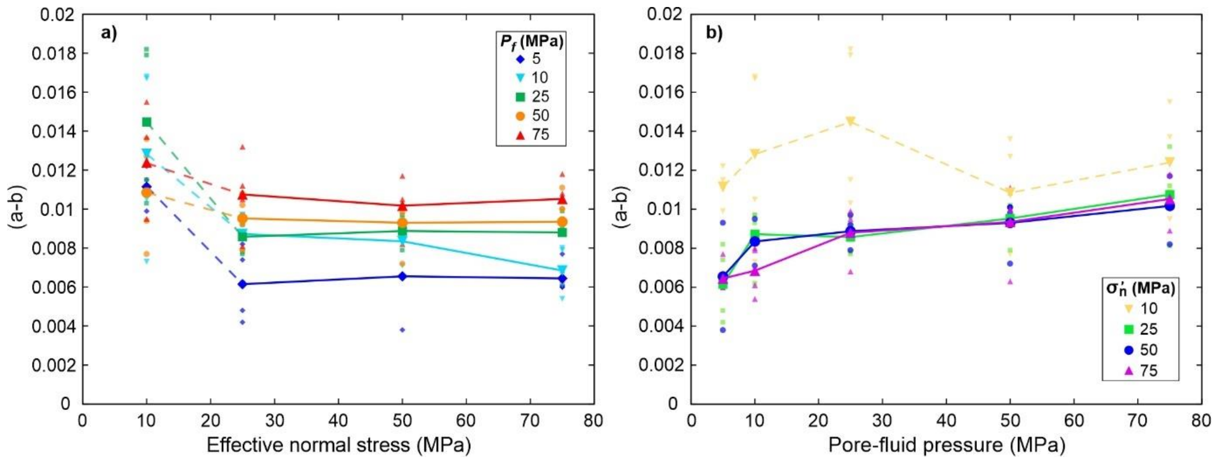

***Figure 4**: The rate-dependence of slip, $(a-b)$, plotted as a function of **a)** effective normal stress and **b)** pore-fluid pressure. Note only the $(a-b)$ values determined from the velocity up-steps (0.3 to 3*

μm·s^{-1}) are shown. Small symbols are all the up-step $(a-b)$ data points calculated from every experiment in this study, with the average $(a-b)$ values for a given experiment shown in bold and connected by contours of constant P_f or σ_n'. The contours are dashed between 10 and 25 MPa effective normal stress as there is a change in the frictional response between these points, with a strong P_f dependence on $(a-b)$ at $\sigma_n' \geq 25$ MPa.

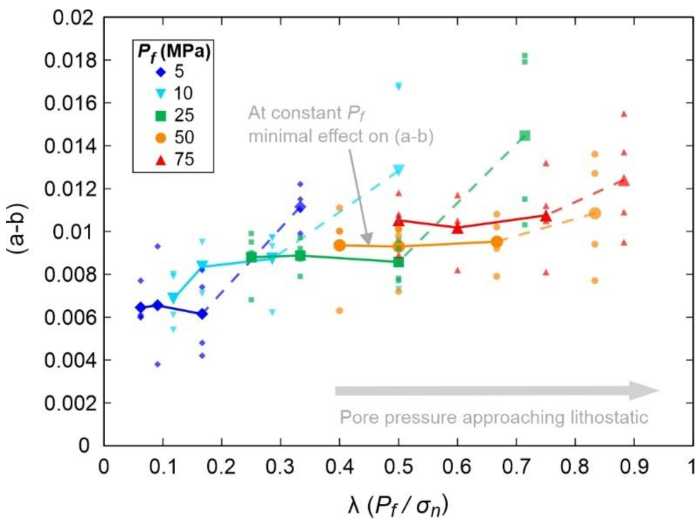

Figure 5: *The rate-dependence of slip, $(a-b)$, plotted as a function of the pore-fluid factor (λ). Note only the $(a-b)$ values determined from the velocity up-steps (0.3 to 3 μm·s^{-1}) are shown. Small symbols are all the up-step $(a-b)$ data points calculated from every experiment in this study, with the average $(a-b)$ values for a given experiment shown in bold and connected by contours of constant P_f. As discussed in the main text, there is a change in the frictional rate-dependence of the Nankai gouge between 10 and 25 MPa effective normal stress, therefore we have dashed the P_f contours between these points (as was also done in Fig. 4).*

To elucidate further the cause of the pore pressure dependence observed in Figure 4, the average up-step values for the individual friction rate parameters a and b are plotted in Figure 6. The friction rate parameter a is always higher than b, leading to the rate-strengthening behaviour observed for Nankai gouge. The data show that the friction rate parameter a is largely independent of the pore-fluid

This manuscript is now published at: https://doi.org/10.1016/j.epsl.2021.117161

pressure (Fig. 6a), with values between 0.006-0.0076 for the entire range of pore-fluid pressures investigated. However, the friction rate parameter b shows a negative dependence on pore-fluid pressure, decreasing from ~0 at $P_f = 5$ MPa, to -0.0032 at $P_f = 75$ MPa (Fig. 6b). There is minimal dependence of the rate parameter b on effective normal stress (and thus also normal stress), further highlighting that changes in b with pore-fluid pressure are responsible for the increased rate-strengthening behaviour (Fig. 6 and Supplementary Fig. 2).

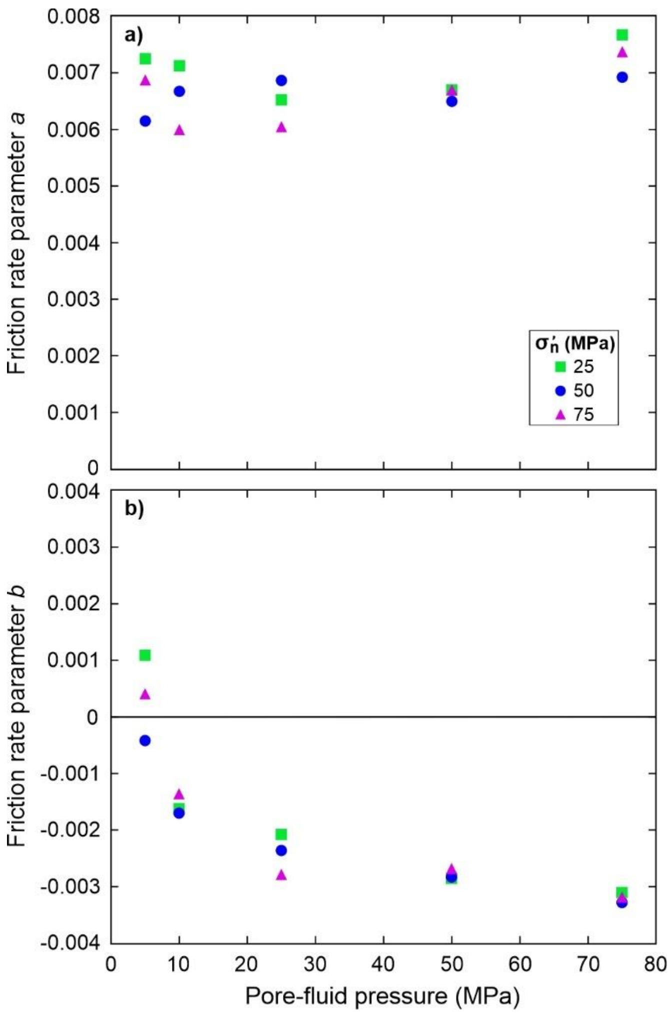

***Figure 6**: Evolution of **a)** the friction rate parameter a, and **b)** the friction rate parameter b as a function of pore-fluid pressure.*

This manuscript is now published at: https://doi.org/10.1016/j.epsl.2021.117161

From the velocity steps in our experiments we can also determine the characteristic slip weakening distance, D_c. Note that although this is termed the 'slip weakening distance', the majority of our velocity steps exhibit a negative evolution effect (i.e., negative b-values, Fig. 6b) and therefore undergo slip-strengthening after an increase in the sliding velocity, rather than weakening. The D_c data are plotted in Figure 7 as a function of (1) effective normal stress at constant pore-fluid pressure, and (2) pore-fluid pressure at constant effective normal stress. The D_c data are more scattered than the $(a - b)$ data in Fig. 4, however there is a general trend of increasing D_c with increasing effective normal stress. We observe no obvious trend between D_c and pore-fluid pressure. There is also no displacement dependent evolution in the D_c data. All of the rate-and-state parameters (a, b and D_c) for each velocity step are reported in Supplementary Tables 1 and 2.

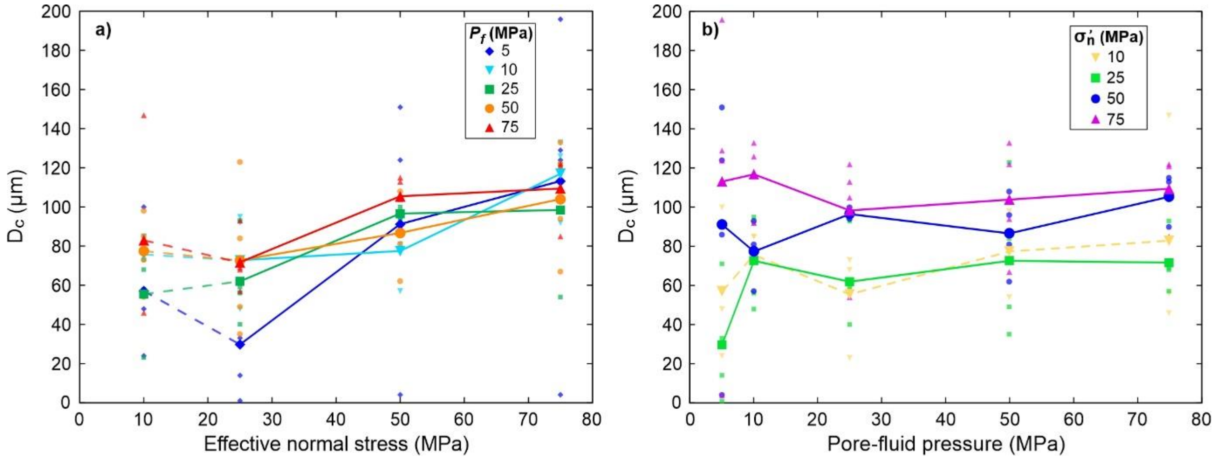

***Figure 7**: The characteristic slip weakening distance, D_c, plotted as a function of **a)** effective normal stress and **b)** pore-fluid pressure. Note only the D_c values determined from the velocity up-steps (0.3 to 3 µm·s^{-1}) are shown. Small symbols are all the up-step D_c data points calculated from every experiment in this study, with the average D_c values for a given experiment shown in bold and connected by contours of constant P_f or σ_n'.*

3.3. Gouge permeability

The permeability of the Nankai gouge measured at the end of each experiment is low, with values in the range of 10^{-21} to 10^{-22} m^2 (Fig. 8). The permeability is dependent on the effective normal stress, with the lowest values occurring at high σ_n'. There does not appear to be any pore-fluid pressure dependence on the measured permeability values (Fig. 8). Given the low permeability of the gouge measured, the possibility of pore fluid pressure transients due to the enhanced compaction rates during velocity steps should be considered (Faulkner et al., 2018). When velocity steps are imposed, the model of Faulkner et al., (2018) predicts an evolution of the rate and state parameters with each successive step, as the effects of excess pore fluid pressure decay with displacement. This behaviour is not observed in our experiments. Consequently, while we cannot rule out some contribution of compaction related pore fluid pressure transients within the gouge layer, the trends of our experimental data suggest that they do not have a significant effect on the frictional parameters obtained.

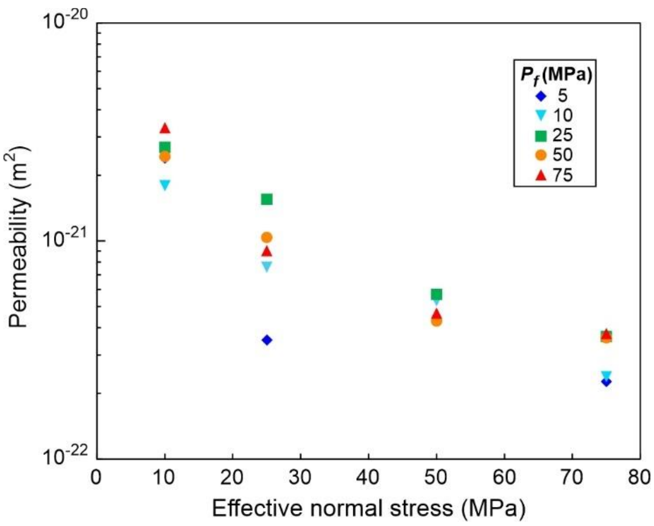

***Figure 8**: Permeability of the Nankai gouge measured at the end of each experiment plotted against effective normal stress. Gouge permeability decreases with increasing effective normal stress.*

This manuscript is now published at: https://doi.org/10.1016/j.epsl.2021.117161

4. Discussion

4.1. The stabilizing effect of pore-fluid pressure on frictional behaviour

The Nankai gouge used in this study is rate-strengthening with $\mu \approx 0.4$, consistent with the majority of previous frictional investigations of fault materials collected from the Nankai Trough (Ikari et al., 2009b; Ikari and Saffer, 2011) and in good agreement with the frictional properties of other clay-bearing materials (e.g. Ikari et al., 2009a; Morrow et al., 2017). The results presented in Figure 4 show that, when $\sigma_n' \geq 25$ MPa, the velocity dependence of Nankai accretionary materials is more sensitive to pore-fluid pressure than effective normal stress, with high P_f leading to higher $(a - b)$ values. In contrast, increasing effective normal stress, and thus also normal stress, has minimal control on $(a - b)$. It should be noted, however, that the characteristic slip weakening distance (D_c) is relatively insensitive to pore-fluid pressure and is more dependent on the effective normal stress (Fig. 7). As the gouge becomes more rate-strengthening at elevated P_f, it can be concluded that pore-fluid pressure has a stabilizing effect on the gouge. This stabilizing effect has been similarly observed in the controlled P_f tests of Xing et al., (2019) on quartz, olivine and serpentine gouges, as well as in studies on frictional behaviour of silty clay input sediments to the Middle America Trench, Costa Rica (Kurzawski et al., 2018), and on illite-quartz mixtures (den Hartog and Spiers, 2013).

The Nankai gouge exhibits a change in frictional rate-dependence between 10 and 25 MPa effective normal stress (Fig. 4), with the pore-pressure dependence of $(a - b)$ only observed for $\sigma_n' \geq 25$ MPa. Previous studies have shown that fault materials can exhibit different frictional properties, in terms of both the overall frictional strength (μ) and the rate-dependence $(a - b)$, at low normal stress, particularly phyllosilicate-bearing gouges. For example, Behnsen and Faulkner (2012) observed a decrease in frictional strength of ten different phyllosilicate gouges as effective normal stress was increased from 5 to 20 MPa, above which the frictional strength remained almost constant. Similar strength behaviour has been observed in other studies on phyllosilicate-bearing gouges (e.g. Ikari et al., 2007; Saffer and Marone, 2003). Ikari et al., (2007) also observed a wide range of $(a - b)$ values at normal stresses below 25 MPa, in comparison to tests they performed above this value. These previous observations of transitions in the frictional properties at low normal stress coincide with the switch in rate-dependent behaviour we observe between 10 and 25 MPa effective normal stress, with pore-fluid pressure exerting the dominant control on the rate-dependence above this value. This could be caused by a different micromechanical response of the gouge at low effective normal stress leading to different frictional behaviour, perhaps as a result of different compaction behaviour (Behnsen and Faulkner, 2012). Regardless of the cause of the switch in behaviour, our results clearly show that $(a-b)$ becomes independent of effective normal stress at $\sigma_n' \geq 25$ MPa (Fig. 4a), with pore-fluid pressure exerting the dominant control on the frictional rate-dependence at these conditions (Fig. 4b).

The results in Figure 6 show that the increase in $(a-b)$ with P_f is caused by a decrease the friction rate parameter b, which becomes more negative at elevated P_f (Fig. 6b). The cause of negative b-values is still not fully understood but they have been widely reported in previous investigations on phyllosilicate-bearing fault materials (e.g. Carpenter et al., 2015; Ikari et al., 2009a; Sánchez-Roa et al., 2017; Scuderi and Collettini, 2018). Ikari et al., (2009a) suggest that in low permeability gouges the effect of dilational hardening immediately after a velocity step, where dilation reduces P_f leading to a local increase in effective normal stress which strengthens the gouge, could be a possible cause of negative b-values. However, they note that there is not much evidence for this in their study as the pore-pressure changes during the velocity steps were too small to cause the negative b-values. Also, if this was the case, the trend of the friction coefficient would actually reduce with time (and slip) as fluid pressure diffused back into the layer, thereby reducing the effective normal stress. Xing et al., (2019) also use dilational hardening as a mechanism to explain the increase in $(a-b)$ they observe with increasing P_f in their study, although it should be noted that all of the b-values they report are positive or near zero. The permeability of the Nankai gouge in our study is sufficiently low (Fig. 8) that transient local pore-pressure perturbations after velocity steps may affect the bulk frictional response of the gouge (Faulkner et al., 2018). However, the permeability of the gouge is predominantly controlled by σ_n' not P_f (Fig. 8). In contrast the negative b-values are largely independent of σ_n' and are controlled by P_f (Fig. 6b). This suggests that although transient pore-pressure variations may affect the frictional response of the gouge they cannot fully explain the cause of the negative b-values and why they become more negative with increasing P_f in our experiments. The model of Faulkner et al., (2018) also indicates that, at the permeabilities measured for the Nankai gouge of this study, any pore-pressure transients would likely be small (<0.5 MPa) and have negligible effect on the friction parameters obtained. This is further evidenced by previous experimental work where positive b-values have been reported for gouges with similarly low permeabilities to the Nankai gouge tested here (e.g. Morrow et al., 2017). Therefore the trends we observe in the velocity dependence of the Nankai gouge, where $(a - b)$ increases with P_f as the b-values decrease, are likely to be primarily a result of the inherent frictional properties of the gouge itself; any transient pore pressure effects that result from the low permeability nature of the gouge will likely only have a secondary effect on the bulk frictional behaviour (Ikari et al., 2009a).

The rate-parameter b is often termed the evolution effect and is classically thought to represent a change in the asperity contact area after a velocity step (Dieterich and Kilgore, 1994; Marone, 1998). Another fundamental manifestation of the evolution effect is the time-dependent increase in frictional strength that occurs when rocks/gouge are held in stationary contact (often termed "frictional aging"), which is also typically attributed to an increase in real contact area as a result of asperity creep (Dieterich and Kilgore, 1994). However, there has been debate in the literature as to whether the contact area hypothesis is the whole story, or whether the contact 'quality' (theory of adhesion; (Bowden and Tabor, 1950)) also affects the frictional properties. In our study we observe mostly negative b-values, which cannot easily be explained using the contact area argument (often colloquially referred to as the "contact quantity" hypothesis). Negative b-values would imply that with slip, the contact area would grow following a velocity up-step. Also, if the evolution of the rate-parameter b were caused by an increase in the real contact area then we would expect to see a dependence on effective normal stress, which we do not observe (Fig. 6b and Supplementary Fig. 2b). Instead we find that the rate-parameter b is dependent on pore-fluid pressure rather than effective normal stress. This observation may therefore support the main alternative hypothesis to explain frictional aging; that it arises from time-dependent chemical bonding on the frictional interface (e.g. Li et al., 2011; Thom et al., 2018), often referred to as the "contact quality" hypothesis. Perhaps at elevated pore-fluid pressure the contact quality at asperities in the gouge changes, potentially decreasing the chemical bonding. One way this might occur is from changes in the properties of structurally bound water layers on the surface of the gouge minerals, which can exert both adhesive and repulsive short-range forces that determine the friction between surfaces (e.g. Israelachvili, 1992). Possibly at high pore-fluid pressure these adsorbed water films evolve in a way that reduces the contact quality leading to the greater negative b-values that we observe in the Nankai gouge materials (Fig. 6b).

Regardless of the cause of pore-pressure dependence on $(a - b)$, and the nature of the underlying mechanism controlling the evolution of the rate-parameter b, it is clear that the gouge becomes more rate-strengthening and thus more stable at high P_f (Fig. 4). Our results show that besides the traditional mechanical effects of P_f, promoting fault slip and lowering the critical stiffness (k_c in Equation 2), it also has a direct influence on the velocity dependence of friction, $(a - b)$. Therefore elevated P_f may promote slip on a fault, but the nature of this slip is likely to be more stable than when P_f is low (as a result of both an increase in $(a - b)$ and reduction in k_c), potentially leading to slow-slip or aseismic creep.

4.2. Implications for fault slip behaviour in subduction zones

Subduction zones exhibit a variety of slip behaviour with depth, including aseismic creep, slow-slip and stick-slip behaviour. It is widely considered that pore-fluid pressure exerts an important control on fault slip behaviour in subduction zones, with elevated pore-fluid pressure often linked to areas of slow-slip (Kodaira et al., 2004; Warren-Smith et al., 2019). At the Nankai Trough it has also been hypothesised that stick-slip behaviour may be suppressed beneath the accretionary wedge by elevated pore-pressures maintaining a low effective normal stress (Tobin and Saffer, 2009). Our results support this hypothesis by demonstrating that elevated pore-fluid pressures actually increase the frictional stability of the fault materials themselves (Figs. 4 and 5), as well as maintain a low effective normal stress on the fault.

The wide array of fault slip behaviour that occurs in subduction zones is often attributed to heterogeneity in both material properties (Barnes et al., 2020; Kirkpatrick et al., 2020) and pore-fluid pressure (Hirose et al., 2021) along the subduction interface. Although the gouge material tested in this study exhibited exclusively rate-strengthening behaviour, previous investigations have shown that rate-weakening material can also be found within the Nankai Trough (e.g. Roesner et al., 2020), suggesting there is a heterogeneous distribution of material properties within the subduction zone. Based on the frictional rate-dependence, the material in this study would be expected to experience stable aseismic creep, whereas the material tested by Roesner et al., (2020) could experience unstable stick-slip behaviour, depending on the elastic stiffness of the surrounding materials (Dieterich, 1979; Leeman et al., 2016). Slow-slip often occurs in fault materials in the transitional region between stable and unstable slip (Bedford and Faulkner, 2021; Leeman et al., 2016), when the rate-dependence of friction, $(a-b)$, is close to zero. Along patches of the subduction zone interface where the material properties would otherwise be rate-weakening and promote unstable slip, we hypothesise that elevated pore-fluid pressures could shift these patches into a frictional stability regime where either slow-slip or aseismic creep would become more favourable. In order to determine whether this is possible, future studies should investigate the role of pore-fluid pressure on the stability of rate-weakening materials to see whether they exhibit a transition from rate-weakening to rate-strengthening at elevated pore-pressure, thus truly stabilizing the frictional behaviour.

5. Conclusions

Our results demonstrate that pore-fluid pressure has a stabilizing effect on Nankai accretionary materials, with $(a-b)$ increasing as P_f is increased, whereas effective normal stress has minimal effect on the stability of the simulated fault gouge. The increase in $(a-b)$ at elevated P_f is caused by an evolution in the rate-and-state parameter b which becomes more negative at high P_f. These results have important implications for fault slip behaviour in subduction zones and suggest that regions of elevated

This manuscript is now published at: https://doi.org/10.1016/j.epsl.2021.117161

pore-fluid pressure are more likely to experience slow-slip or aseismic creep than those where the pore-fluid pressure is low.

Acknowledgments

This work used samples and shipboard data collected during Integrated Ocean Drilling Program (IODP) Expedition 358. We would like to thank the crew and the technicians (Marine Works Japan) of D/V Chikyu for their effort and support during the expedition. We thank Gary Coughlan for his assistance in developing and maintaining the experimental equipment. We are grateful to James Utley for help with XRD analysis. We also thank Matt Ikari and Marco Scuderi for constructive reviews that improved the clarity of the manuscript. This work is supported by Natural Environment Research Council grants NE/S015531/1 and NE/P002943/1. The data reported in the figures can be accessed in National Geoscience Data Centre (NGDC) data repository: https://webapps.bgs.ac.uk/services/ngdc/accessions/index.html#item163985

References

Ando, M., 1975. Source mechanisms and tectonic significance of historical earthquakes along the Nankai Trough, Japan. Tectonophysics 27, 119–140. https://doi.org/https://doi.org/10.1016/0040-1951(75)90102-X

Araki, E., Saffer, D.M., Kopf, A.J., Wallace, L.M., Kimura, T., Machida, Y., Ide, S., Davis, E., Scientists, I.E. 365 shipboard, 2017. Recurring and triggered slow-slip events near the trench at the Nankai Trough subduction megathrust. Science. 356, 1157–1160. https://doi.org/10.1126/science.aan3120

Barnes, P.M., Wallace, L.M., Saffer, D.M., Bell, R.E., Underwood, M.B., Fagereng, A., Meneghini, F., Savage, H.M., Rabinowitz, H.S., Morgan, J.K., Kitajima, H., Kutterolf, S., Hashimoto, Y., Engelmann De Oliveira, C.H., Noda, A., Crundwell, M.P., Shepherd, C.L., Woodhouse, A.D.,

This manuscript is now published at: https://doi.org/10.1016/j.epsl.2021.117161

Harris, R.N., Wang, M., Henrys, S., Barker, D.H.N., Petronotis, K.E., Bourlange, S.M., Clennell, M.B., Cook, A.E., Dugan, B.E., Elger, J., Fulton, P.M., Gamboa, D., Greve, A., Han, S., Hupers, A., Ikari, M.J., Ito, Y., Kim, G.Y., Koge, H., Lee, H., Li, X., Luo, M., Malie, P.R., Moore, G.F., Mountjoy, J.J., McNamara, D.D., Paganoni, M., Screaton, E.J., Shankar, U., Shreedharan, S., Solomon, E.A., Wang, X., Wu, H.-Y., Pecher, I.A., LeVay, L.J., Scientists, I.E. 372, 2020. Slow slip source characterized by lithological and geometric heterogeneity. Sci. Adv. 6. https://doi.org/10.1126/sciadv.aay3314

Bedford, J.D., Faulkner, D.R., 2021. The role of grain size and effective normal stress on localization and the frictional stability of simulated quartz gouge. Geophys. Res. Lett. 48, e2020GL092023. https://doi.org/10.1029/2020gl092023

Beeler, N.M., Tullis, T.E., Blanpied, M.L., Weeks, J.D., 1996. Frictional behavior of large displacement experimental faults. J. Geophys. Res. 101, 8697–8715.

Behnsen, J., Faulkner, D.R., 2012. The effect of mineralogy and effective normal stress on frictional strength of sheet silicates. J. Struct. Geol. 42, 49–61. https://doi.org/10.1016/j.jsg.2012.06.015

Bowden, F.P., Tabor, D., 1950. The friction and lubrication of solids, Part I. Clarendon Press, Oxford.

Brace, W.F., Walsh, J.B., Frangos, W.T., 1968. Permeability of granite under high pressure. J. Geophys. Res. 73, 2225–2236. https://doi.org/10.1029/JB073i006p02225

Byerlee, J., 1978. Friction of Rocks. Pure Appl. Geophys. 116, 615–626. https://doi.org/https://doi.org/10.1007/BF00876528

Carpenter, B.M., Collettini, C., Viti, C., Cavallo, A., 2016. The influence of normal stress and sliding velocity on the frictional behaviour of calcite at room temperature: insights from laboratory experiments and microstructural observations. Geophys. J. Int. 205, 548–561. https://doi.org/10.1093/gji/ggw038

Carpenter, B.M., Saffer, D.M., Marone, C., 2015. Frictional properties of the active San Andreas Fault at SAFOD: Implications for fault strength and slip behavior. J. Geophys. Res. Solid Earth

This manuscript is now published at: https://doi.org/10.1016/j.epsl.2021.117161

120, 5273–5289. https://doi.org/10.1002/2015JB011963

Carpenter, B.M., Saffer, D.M., Marone, C., 2012. Frictional properties and sliding stability of the San Andreas fault from deep drill core. Geology 40, 759–762. https://doi.org/10.1130/G33007.1

den Hartog, S.A.M., Spiers, C.J., 2013. Influence of subduction zone conditions and gouge composition on frictional slip stability of megathrust faults. Tectonophysics 600, 75–90. https://doi.org/10.1016/j.tecto.2012.11.006

Dieterich, J.H., 1979. Modeling of rock friction 1. Experimental results and constitutive equations. J. Geophys. Res. 84, 2161–2168. https://doi.org/https://doi.org/10.1029/JB084iB05p02161

Dieterich, J.H., Kilgore, B.D., 1994. Direct observation of frictional contacts: New insights for state-dependent properties. Pure Appl. Geophys. 143, 283–302. https://doi.org/https://doi.org/10.1007/BF00874332

Faulkner, D.R., Armitage, P.J., 2013. The effect of tectonic environment on permeability development around faults and in the brittle crust. Earth Planet. Sci. Lett. 375, 71–77. https://doi.org/10.1016/j.epsl.2013.05.006

Faulkner, D.R., Rutter, E.H., 1998. The gas permeability of clay-bearing fault gorge at 20°C. Geol. Soc. London, Spec. Publ. 147, 147–156. https://doi.org/10.1144/GSL.SP.1998.147.01.10

Faulkner, D.R., Sanchez-Roa, C., Boulton, C., den Hartog, S.A.M., 2018. Pore fluid pressure development in compacting fault gouge in theory, experiments, and nature. J. Geophys. Res. Solid Earth 123, 226–241. https://doi.org/10.1002/2017JB015130

Giorgetti, C., Carpenter, B.M., Collettini, C., 2015. Frictional behavior of talc-calcite mixtures. J. Geophys. Res. Solid Earth 120, 6614–6633. https://doi.org/10.1002/2015JB011970

Hillier, S., 2000. Accurate quantitative analysis of clay and other minerals in sandstones by XRD: comparison of a Rietveld and a reference intensity ratio (RIR) method and the importance of sample preparation. Clay Miner. 35, 291–302. https://doi.org/10.1180/000985500546666

Hirose, T., Hamada, Y., Tanikawa, W., Kamiya, N., Yamamoto, Y., Tsuji, T., Kinoshita, M., Heuer, B., Inagaki, F., Morono, Y., Kubo, Y., 2021. High fluid-pressure patches beneath the décollement: A potential source of slow earthquakes in the Nankai Trough off Cape Muroto. J. Geophys. Res. Solid Earth 126, e2021JB021831. https://doi.org/https://doi.org/10.1029/2021JB021831

Ikari, M.J., Kopf, A.J., 2017. Seismic potential of weak, near-surface faults revealed at plate tectonic slip rates. Sci. Adv. 3. https://doi.org/10.1126/sciadv.1701269

Ikari, M.J., Marone, C., Saffer, D.M., 2011. On the relation between fault strength and frictional stability. Geology 39, 83–86. https://doi.org/10.1130/G31416.1

Ikari, M.J., Saffer, D.M., 2011. Comparison of frictional strength and velocity dependence between fault zones in the Nankai accretionary complex. Geochemistry Geophys. Geosystems 12. https://doi.org/10.1029/2010GC003442

Ikari, M.J., Saffer, D.M., Marone, C., 2009a. Frictional and hydrologic properties of clay-rich fault gouge. J. Geophys. Res. 114. https://doi.org/10.1029/2008JB006089

Ikari, M.J., Saffer, D.M., Marone, C., 2009b. Frictional and hydrologic properties of a major splay fault system, Nankai subduction zone. Geophys. Res. Lett. 36, L20313. https://doi.org/10.1029/2009GL040009

Ikari, M.J., Saffer, D.M., Marone, C., 2007. Effect of hydration state on the frictional properties of montmorillonite-based fault gouge. J. Geophys. Res. Solid Earth 112, B06423. https://doi.org/10.1029/2006JB004748

Israelachvili, J.N., 1992. Adhesion forces between surfaces in liquids and condensable vapours. Surf. Sci. Rep. 14, 109–159. https://doi.org/10.1016/0167-5729(92)90015-4

Ito, Y., Obara, K., 2006. Dynamic deformation of the accretionary prism excites very low frequency earthquakes. Geophys. Res. Lett. 33. https://doi.org/10.1029/2005GL025270

Kimura, G., Kitamura, Y., Hashimoto, Y., Yamaguchi, A., Shibata, T., Ujiie, K., Okamoto, S., 2007.

Transition of accretionary wedge structures around the up-dip limit of the seismogenic subduction zone. Earth Planet. Sci. Lett. 255, 471–484. https://doi.org/10.1016/j.epsl.2007.01.005

Kinoshita, M., Tobin, H., Ashi, J., Kimura, G., Lallemant, S., Screaton, E.J., Curewitz, D., Masago, H., Moe, K.T., Scientists, E. 314/315/316, 2009. Proceedings of the Integrated Drilling Program Expeditions 314/315/316. Integrated Ocean Drilling Program Management International, Inc. https://doi.org/doi:10.2204/iodp.proc.314315316.2009.

Kirkpatrick, J.D., Edwards, J.H., Verdecchia, A., Kluesner, J.W., Harrington, R.M., Silver, E.A., 2020. Subduction megathrust heterogeneity characterized from 3D seismic data. Nat. Geosci. 13, 369–374. https://doi.org/10.1038/s41561-020-0562-9

Kitajima, H., Hirose, T., Ikari, M., Kanagawa, K., Kimura, G., Kinoshita, M., Saffer, D., Tobin, H., Yamaguchi, A., Eguchi, N., Maeda, L., Toczko, S., Scientists, E. 358, 2020. Site C0002, in: Tobin, H., Hirose, T., Ikari, M., Kanagawa, K., Kimura, G., Kinoshita, M., Kitajima, H., Saffer, D., Yamaguchi, A., Eguchi, N., Maeda, L., Toczko, S., Scientists, E. 358 (Eds.), NanTroSEIZE Plate Boundary Deep Riser 4: Nankai Seismogenic/Slow Slip Megathrust. Proceedings of the International Ocean Discovery Program, 358, College Station, TX. https://doi.org/https://doi.org/10.14379/iodp.proc.358.103.2020

Kodaira, S., Iidaka, T., Kato, A., Park, J.-O., Iwasaki, T., Kaneda, Y., 2004. High pore fluid pressure may cause silent slip in the Nankai Trough. Science. 304, 1295–1298. https://doi.org/10.1126/science.1096535

Kurzawski, R.M., Niemeijer, A.R., Stipp, M., Charpentier, D., Behrmann, J.H., Spiers, C.J., 2018. Frictional properties of subduction input sediments at an erosive convergent continental margin and related controls on décollement slip modes: The Costa Rica Seismogenesis Project. J. Geophys. Res. Solid Earth 123, 8385–8408. https://doi.org/10.1029/2017JB015398

Kurzawski, R.M., Stipp, M., Niemeijer, A.R., Spiers, C.J., Behrmann, J.H., 2016. Earthquake nucleation in weak subducted carbonates. Nat. Geosci. 9, 717–722.

This manuscript is now published at: https://doi.org/10.1016/j.epsl.2021.117161

https://doi.org/10.1038/NGEO2774

Leeman, J.R., Saffer, D.M., Scuderi, M.M., Marone, C., 2016. Laboratory observations of slow earthquakes and the spectrum of tectonic fault slip modes. Nat. Commun. 7. https://doi.org/10.1038/ncomms11104

Li, Q., Tullis, T.E., Goldsby, D., Carpick, R.W., 2011. Frictional ageing from interfacial bonding and the origins of rate and state friction. Nature 480, 233–236. https://doi.org/10.1038/nature10589

Mair, K., Marone, C., 1999. Friction of simulated fault gouge for a wide range of velocities and normal stresses. J. Geophys. Res. 104, 28899–28914. https://doi.org/https://doi.org/10.1029/1999JB900279

Marone, C., 1998. Laboratory-derived friction laws and their application to seismic faulting. Annu. Rev. Earth Planet. Sci. 26, 643–696.

Marone, C., Raleigh, C.B., Scholz, C.H., 1990. Frictional behavior and constitutive modeling of simulated fault gouge. J. Geophys. Res. 95, 7007–7025. https://doi.org/https://doi.org/10.1029/JB095iB05p07007

Mizutani, T., Hirauchi, K., Lin, W., Sawai, M., 2017. Depth dependence of the frictional behavior of montmorillonite fault gouge: Implications for seismicity along a décollement zone. Geophys. Res. Lett. 44, 5383–5390. https://doi.org/10.1002/2017GL073465

Morrow, C.A., Moore, D.E., Lockner, D.A., 2017. Frictional strength of wet and dry montmorillonite. J. Geophys. Res. Solid Earth 122, 3392–3409. https://doi.org/10.1002/2016JB013658

Niemeijer, A.R., Collettini, C., 2014. Frictional properties of a low-angle normal fault under in situ conditions: Thermally-activated velocity weakening. Pure Appl. Geophys. 171, 2641–2664. https://doi.org/10.1007/s00024-013-0759-6

Numelin, T., Marone, C., Kirby, E., 2007. Frictional properties of natural fault gouge from a low-angle normal fault, Panamint Valley, California. Tectonics 26. https://doi.org/10.1029/2005TC001916

Okamoto, A.S., Niemeijer, A.R., Takeshita, T., Verberne, B.A., Spiers, C.J., 2020. Frictional properties of actinolite-chlorite gouge at hydrothermal conditions. Tectonophysics 779. https://doi.org/10.1016/j.tecto.2020.228377

Okamoto, A.S., Verberne, B.A., Niemeijer, A.R., Takahashi, M., Shimizu, I., Ueda, T., Spiers, C.J., 2019. Frictional properties of simulated chlorite gouge at hydrothermal conditions: Implications for subduction megathrusts. J. Geophys. Res. Solid Earth 124, 4545–4565. https://doi.org/10.1029/2018JB017205

Okuda, H., Katayama, I., Sakuma, H., Kawai, K., 2021. Effect of normal stress on the frictional behavior of brucite: application to slow earthquakes at the subduction plate interface in the mantle wedge. Solid Earth 12, 171–186. https://doi.org/10.5194/se-12-171-2021

Park, J.-O., Tsuru, T., Kodaira, S., Cummins, P.R., Kaneda, Y., 2002. Splay fault branching along the Nankai Subduction Zone. Science. 297, 1157–1160. https://doi.org/10.1126/science.1074111

Rabinowitz, H.S., Savage, H.M., Skarbek, R.M., Ikari, M.J., Carpenter, B.M., Collettini, C., 2018. Frictional behavior of input sediments to the Hikurangi Trench, New Zealand. Geochemistry Geophys. Geosystems 19, 2973–2990. https://doi.org/10.1029/2018GC007633

Rathbun, A.P., Marone, C., 2013. Symmetry and the critical slip distance in rate and state friction laws. J. Geophys. Res. Solid Earth 118, 3728–3741. https://doi.org/10.1002/jgrb.50224

Roesner, A., Ikari, M.J., Saffer, D.M., Stanislowski, K., Eijsink, A.M., Kopf, A.J., 2020. Friction experiments under in-situ stress reveal unexpected velocity-weakening in Nankai accretionary prism samples. Earth Planet. Sci. Lett. 538. https://doi.org/10.1016/j.epsl.2020.116180

Saffer, D.M., Frye, K.M., Marone, C., Mair, K., 2001. Laboratory results indicating complex and potentially unstable frictional behavior of smectite clay. Geophys. Res. Lett. 28, 2297–2300. https://doi.org/https://doi.org/10.1029/2001GL012869

Saffer, D.M., Marone, C., 2003. Comparison of smectite- and illite-rich gouge frictional properties: application to the updip limit of the seismogenic zone along subduction megathrusts. Earth

Planet. Sci. Lett. 215, 219–235. https://doi.org/10.1016/S0012-821X(03)00424-2

Saffer, D.M., Tobin, H.J., 2011. Hydrogeology and mechanics of subduction zone forearcs: Fluid flow and pore pressure. Annu. Rev. Earth Planet. Sci. 39, 157–186. https://doi.org/10.1146/annurev-earth-040610-133408

Sánchez-Roa, C., Faulkner, D.R., Boulton, C., Jimenez-Millan, J., Nieto, F., 2017. How phyllosilicate mineral structure affects fault strength in Mg-rich fault systems. Geophys. Res. Lett. 44, 5457–5467. https://doi.org/10.1002/2017GL073055

Sawai, M., Niemeijer, A.R., Plümper, O., Hirose, T., Spiers, C.J., 2016. Nucleation of frictional instability caused by fluid pressurization in subducted blueschist. Geophys. Res. Lett. 43, 2543–2551. https://doi.org/10.1002/2015GL067569

Scholz, C.H., 1998. Earthquakes and friction laws. Nature 391, 37–42. https://doi.org/https://doi.org/10.1038/34097

Scruggs, V.J., Tullis, T.E., 1998. Correlation between velocity dependence of friction and strain localization in large displacement experiments on feldspar, muscovite and biotite gouge. Tectonphysics 295, 15–40. https://doi.org/https://doi.org/10.1016/S0040-1951(98)00113-9

Scuderi, M.M., Collettini, C., 2018. Fluid injection and the mechanics of frictional stability of shale-bearing faults. J. Geophys. Res. Solid Earth 123, 8364–8384. https://doi.org/10.1029/2018JB016084

Scuderi, M.M., Collettini, C., 2016. The role of fluid pressure in induced vs. triggered seismicity: insights from rock deformation experiments on carbonates. Sci. Rep. 6. https://doi.org/10.1038/srep24852

Scuderi, M.M., Niemeijer, A.R., Collettini, C., Marone, C., 2013. Frictional properties and slip stability of active faults within carbonate-evaporite sequences: The role of dolomite and anhydrite. Earth Planet. Sci. Lett. 369–370, 220–232. https://doi.org/10.1016/j.epsl.2013.03.024

Seno, T., Stein, S., Gripp, A.E., 1993. A model for the motion of the Philippine Sea Plate consistent

This manuscript is now published at: https://doi.org/10.1016/j.epsl.2021.117161

with NUVEL-1 and geological data. J. Geophys. Res. 98, 17941–17948. https://doi.org/https://doi.org/10.1029/93JB00782

Skarbek, R.M., Savage, H.M., 2019. RSFit3000 : A MATLAB GUI-based program for determining rate and state frictional parameters from experimental data. Geosphere 15, 1665–1676. https://doi.org/https://doi.org/10.1130/GES02122.1

Smith, S.A.F., Faulkner, D.R., 2010. Laboratory measurements of the frictional properties of the Zuccale low-angle normal fault, Elba Island, Italy. J. Geophys. Res. 115, B02407. https://doi.org/10.1029/2008JB006274

Sugioka, H., Okamoto, T., Nakamura, T., Ishihara, Y., Ito, A., Obana, K., Kinoshita, M., Nakahigashi, K., Shinohara, M., Fukao, Y., 2012. Tsunamigenic potential of the shallow subduction plate boundary inferred from slow seismic slip. Nat. Geosci. 5, 414–418. https://doi.org/10.1038/ngeo1466

Terzaghi, K., 1943. Theoretical soil mechanics. New York: Wiley, 1943.

Thom, C.A., Carpick, R.W., Goldsby, D.L., 2018. Constraints on the physical mechanism of frictional aging from nanoindentation. Geophys. Res. Lett. 45, 13306–13311. https://doi.org/10.1029/2018GL080561

Tobin, H., Hirose, T., Ikari, M., Kanagawa, K., Kimura, G., Kinoshita, M., Kitajima, H., Saffer, D., Yamaguchi, A., Eguchi, N., Maeda, L., Toczko, S., Scientists, E. 358, 2020. Expedition 358 summary, in: Tobin, H., Hirose, T., Ikari, M., Kanagawa, K., Kimura, G., Kinoshita, M., Kitajima, H., Saffer, D., Yamaguchi, A., Eguchi, N., Maeda, L., Toczko, S., Scientists, E. 358 (Eds.), NanTroSEIZE Plate Boundary Deep Riser 4: Nankai Seismogenic/Slow Slip Megathrust. Proceedings of the International Ocean Discovery Program, 358, College Station, TX. https://doi.org/https://doi.org/10.14379/iodp.proc.358.101.2020

Tobin, H.J., Kinoshita, M., 2006. NanTroSEIZE: The IODP Nankai Trough Seismogenic Zone Experiment. Sci. Drill. 2, 23–27. https://doi.org/10.2204/iodp.sd.2.06.2006

Tobin, H.J., Saffer, D.M., 2009. Elevated fluid pressure and extreme mechanical weakness of a plate boundary thrust, Nankai Trough subduction zone. Geology 37, 679–682. https://doi.org/10.1130/G25752A.1

Tsutsumi, A., Fabbri, O., Karpoff, A.M., Ujiie, K., Tsujimoto, A., 2011. Friction velocity dependence of clay-rich fault material along a megasplay fault in the Nankai subduction zone at intermediate to high velocities. Geophys. Res. Lett. 38. https://doi.org/10.1029/2011GL049314

Ujiie, K., Tsutsumi, A., 2010. High-velocity frictional properties of clay-rich fault gouge in a megasplay fault zone, Nankai subduction zone. Geophys. Res. Lett. 37. https://doi.org/10.1029/2010GL046002

Warren-Smith, E., Fry, B., Wallace, L., Chon, E., Henrys, S., Sheehan, A., Mochizuki, K., Schwartz, S., Webb, S., Lebedev, S., 2019. Episodic stress and fluid pressure cycling in subducting oceanic crust during slow slip. Nat. Geosci. 12, 475–481. https://doi.org/10.1038/s41561-019-0367-x

Xing, T., Zhu, W., French, M., Belzer, B., 2019. Stabilizing effect of high pore fluid pressure on slip behaviors of gouge-bearing faults. J. Geophys. Res. Solid Earth 124, 9526–9545. https://doi.org/10.1029/2019JB018002